Snowball Earth: A thin-ice solution with flowing sea glaciers

David Pollard and James F. Kasting

Department of Geosciences, Earth and Environmental Systems Institute, Pennsylvania State University, University Park, Pennsylvania, USA

Received 11 June 2004; revised 16 March 2005; accepted 28 March 2005; published 16 July 2005.

[1] The late Neoproterozoic era, ~600–800 Myr ago, was marked by at least two intervals of widespread cold that left glacial deposits at low paleolatitudes. Both "Snowball" solutions with global ice cover and "Slushball" solutions with ice-free tropical oceans have been proposed to explain the paleomagnetic data. The Snowball model is best able to explain the auxiliary geological evidence, particularly the existence of cap carbonates, but it implies drastic survival pressure on the photosynthetic biota if the ice cover was everywhere thick enough to prevent sunlight from reaching the underlying ocean. A "thin ice" solution that avoids this problem has been proposed but is thought to be inconsistent with realistic optical properties of sea ice and with the equatorward flow of sea glaciers. Here we use a coupled energy-balance climate/sea-glacier model to argue that these apparent difficulties can be overcome and that thin tropical ice may have prevailed during these remarkable glacial episodes. We also suggest that (1) some processes beyond the scope of zonal mean energy-balance models may significantly affect the solutions and (2) thin ice could have prevailed on low-latitude seas (or large lakes) protected from large-scale sea-glacier flow by surrounding land even if most of the Earth was in a "hard Snowball" state.

Citation: Pollard, D., and J. F. Kasting (2005), Snowball Earth: A thin-ice solution with flowing sea glaciers, *J. Geophys. Res.*, *110*, C07010, doi:10.1029/2004JC002525.

1. Introduction

[2] The Snowball Earth model for the Neoproterozoic glaciations, proposed initially by *Kirschvink* [1992] and further elaborated by *Hoffman et al.* [1998], suggests that the entire Earth was ice-covered at ~750 Myr ago and again at ~600 Myr ago. This hypothesis is consistent with the predictions of energy-balance climate models (EBMs) with simple meridional heat transport [*Budyko*, 1969; *Sellers*, 1969; *Caldeira and Kasting*, 1992] and with some more complex intermediate and general circulation models (GCMs) [*Jenkins*, 2000; *Donnadieu et al.*, 2003, 2004a, 2004b; *Pollard and Kasting*, 2004; *Pierrehumbert*, 2004]. Such models predict that sea ice should quickly blanket the tropics once the ice line moves equatorward of 25–30 degrees latitude. Typically, this instability sets in at atmospheric CO_2 concentrations similar to or somewhat lower than today, given a solar constant of ~0.94 times today's value. This is approximately the value of the solar constant predicted at 600 Myr ago [*Gough*, 1981]. Not all climate models exhibit this same climate sensitivity, however. EBMs in which heat transport across the ice line is inhibited are more resistant to global glaciation because the tropics cannot export heat to higher latitudes [*Lindzen and Farrell*, 1977]. Rapid meridional heat exchange within the tropics delays the onset of global glaciation to a lesser extent [*Lindzen and Farrell*, 1977]. Coupled atmosphere-ocean GCMs also appear to be resistant to global glaciation, apparently because of rapid deep-ocean convection in the ice-free subtropics [*Poulsen et al.*, 2001; *Poulsen*, 2003]. Hence climate models remain ambiguous as to the precise conditions needed to trigger a Snowball Earth.

[3] "Slushball" models with ice-free tropical oceans are also capable, in principle, of explaining low-latitude glaciation. *Hyde et al.* [2000] demonstrated that continental glaciers formed at high elevations on a tropically situated continent could have flowed down to an unfrozen ocean, thereby explaining the existence of dropstones in Australian marine sediments. However, neither this model, nor others like it [*Poulsen*, 2003], explains the existence of cap carbonates. Both Neoproterozoic glacial layers are overlain by several meters of finely grained carbonate rock that is thought to have been deposited in the immediate aftermath of the glaciation. For the Marinoan (~600 Ma) glaciation in Svalbard, the cap dolostone is 3–18 m thick [*Halverson et al.*, 2004]. In the Snowball Earth model, these cap carbonates are formed by removal of volcanic CO_2 that accumulated during the glaciations and provided the greenhouse warming needed to escape them. The rate of formation is exceptionally rapid because the ice retreats within a few hundred years once the critical threshold for meltback is reached and because the ensuing high surface temperatures and high CO_2 partial pressures cause the carbonate-silicate cycle to be wildly out of balance. In the Slushball model, by contrast, the ice should retreat slowly (millions to tens of millions of years) because the ice line remains in quasi–steady state as CO_2 accumulates. Non-Snowball mecha-

0148-0227/05/2004JC002525$09.00

nisms have been proposed to explain these cap carbonates [*Kennedy et al.*, 2001; *Jiang et al.*, 2003; *Ridgewell et al.*, 2003]. However, none of these models explains the unique, conformable interbedding of carbonates and glacial deposits, along with the massive amount of carbonate in the caps. In the Snowball Earth model, by contrast, the existence of cap carbonates with these essential characteristics is virtually unavoidable.

[4] The major drawback of the Snowball Earth model is that it is difficult to understand how photosynthetic algae and other phototrophic organisms could have survived such a catastrophe [*Knoll*, 2003]. If the ice thickness was determined strictly by geothermal heat flow, then the ice should have been a kilometer or more thick everywhere, and no sunlight should have been transmitted through it. The ice thickness, Δz, in this "hard Snowball" model is given by

$$\Delta z = \frac{k \Delta T}{F_g}, \tag{1}$$

where k is the thermal conductivity of ice ($\sim$2.5 W m^{-1} K^{-1}), F_g is the geothermal heat flux ($\sim$0.06 W m^{-2}), and ΔT is the temperature difference between the atmosphere and the seawater beneath the ice. Using numbers from the *Hyde et al.* [2000] hard Snowball model, the tropical surface temperature is -27°C. Thus, if seawater freezes at -2°C, as today, $\Delta T = 25$°C, and the ice thickness is $\sim$1000 m. The average geothermal heat flux may have been slightly higher in the Neoproterozoic but not enough to alter the basic argument. A possible Paleoproterozoic Snowball Earth at 2.3 Ga [*Evans et al.*, 1997] would have had ice that was 2–3 times thinner as a consequence of the significantly higher geothermal heat flow at that time.

[5] The ice thickness in this "hard Snowball" model can be reduced to $\sim$100 m in the tropics by sublimation at the ice surface, accompanied by refreezing at the base, but this is still much too thick to allow sunlight to penetrate. Various workers have suggested that refugia would still have been available in brine channels, tropical polynyas, tidal cracks, meltwater ponds, and shallow hot springs around volcanic islands [*Hoffman and Schrag*, 2002]. *Hoffman and Schrag* [2000] have even suggested that such a severe restriction on available habitats could have spurred evolution and might account for the emergence of multicellular plants and animals just prior to the Cambrian, $\sim$560 Myr ago. It is difficult to demonstrate conclusively that this idea is incorrect. However, the roughly 40-Myr time lag between the end of the last Neoproterozoic Snowball Earth episode and the Cambrian explosion suggests that these two events are causally unrelated. Furthermore, to our knowledge there is no evidence for major biological extinctions associated with the Neoproterozoic glacial events. A Snowball Earth model with more modest biological consequences might therefore be easier to reconcile with the phylogenetic and fossil record.

[6] A biologically friendlier "thin ice" model for Snowball Earth has been suggested by *McKay* [2000]. (The term "thin ice" refers to the few-meter thickness and transparency of the ice, with no glacial dynamic connotations.) Lakes in the dry valleys of Antarctica support a thriving photosynthetic biota living beneath $\sim$5 m of perennial ice. This is possible because ice that is free of bubbles and other scatterers is exceptionally transparent to visible and UV radiation shortward of $\sim$700 nm [*Warren et al.*, 2002]. In the Antarctic lakes the heat that keeps the lakes from freezing more deeply is provided by inflow of summer meltwater. On Snowball Earth the required heat could have been provided by sunlight itself [*McKay*, 2000]. However, the thin ice solution is currently considered not to be viable, partly because modern sea ice is bubbly, and hence highly opaque [*Warren et al.*, 2002], and partly because thick sea ice (or "sea glaciers") [*Warren et al.*, 2002] should have flowed from high latitudes down into the tropics [*Goodman and Pierrehumbert*, 2003]. Specifically, *Warren et al.* [2002] argued that tropical sea ice must have had a high albedo, and hence lots of bubbles, in order to keep the surface cold, in which case it could not have transmitted enough sunlight to keep the ice thin. According to their analysis, the only solutions for the tropical ocean are either thick (opaque) ice or none at all. Below, we demonstrate that this is not necessarily the case.

[7] To re-examine this issue, we constructed a seasonal energy-balance climate model (EBM) with fully coupled sea-glacier dynamics, and applied it to a zonally symmetric all-ocean planet (Figure 1; a detailed model description is given in Appendix A). The EBM includes standard diffusive poleward heat transport, but with separate explicit components for atmosphere, ocean, snow and ice, as demanded by the problem at hand. The ice component includes relatively accurate treatments of penetrating solar radiation and internal ice temperatures. The most important free parameter is the visible single scattering albedo of ice, ω_0, which depends on the density of bubbles and brine inclusions. We used this EBM to simulate a variety of different Snowball Earth-type scenarios with and without sea-glacier flow, and with various values of single-scattering albedo.

[8] Sections 2 and 3 present results for our nominal model version, which was designed to capture only those physical processes that are essential for sea glaciers and Snowball Earth. (We note parenthetically that the term "sea glaciers," first used by *Warren et al.* [2002], is appropriate because this ice is not only much thicker than contemporary sea ice, but also contains much less salt because of the manner in which it forms. Hence its dynamical behavior should be more like that of terrestrial, glacial ice than of modern sea ice. Furthermore, although sea glaciers flow like modern floating ice shelves, they have very different origins, with ice shelves supplied by continental ice sheets.) We show that sea glaciers and thin tropical ice can indeed coexist, provided that the near-surface ice is sufficiently clear (section 4). However, we show in section 6 that some neglected processes may in fact be important, with the potential to significantly affect thin-ice results for the open ocean. In section 7 we conclude that EBM modeling can only hint at the viability of thin ice during full Snowball episodes and that more comprehensive 3-D GCMs with interactive ice components will be needed to resolve the issue.

2. Results: Ice Extent Versus CO_2

[9] We began by examining the effect of sea-glacier dynamics on the transition from Slushball to Snowball

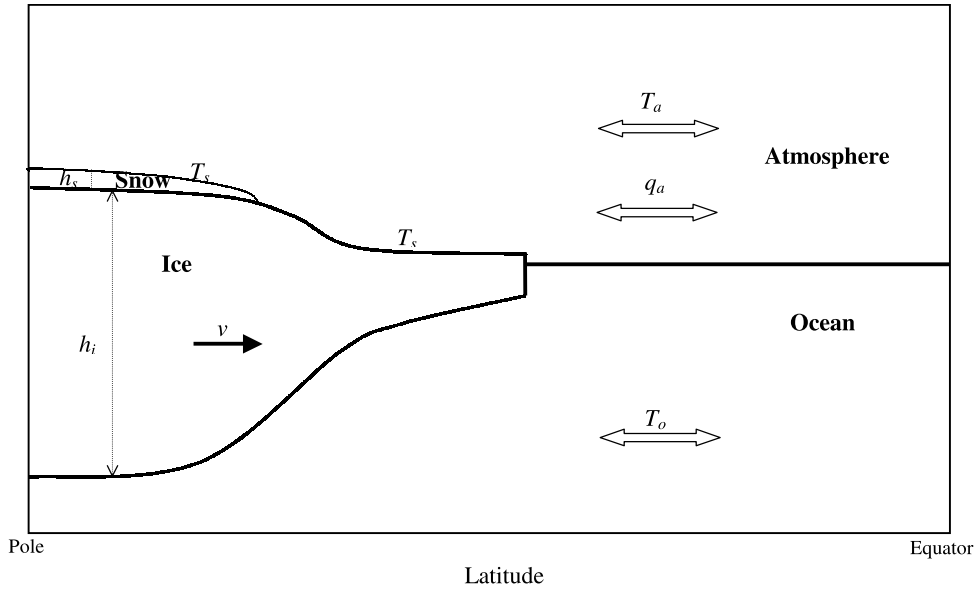

Figure 1. Schematic diagram of the coupled climate and sea-glacier model. All prognostic variables are shown: T_a, atmospheric temperature; q_a, atmospheric specific humidity; T_s, surface (seasonal layer) temperature of snow or ice; T_o, ocean 50-m mixed layer temperature; h_s, snow thickness; h_i, ice thickness. Also shown is the (diagnostic) sea-glacier ice velocity v. Although only one hemisphere is shown here, the model domain is global, which is necessary to properly capture seasonal cycles. (Since annual mean results are all hemispherically symmetric, they can be shown over one hemisphere, as in other figures below). The model is described fully in Appendix A.

Earth. Specifically, we wanted to test whether they could have overwhelmed the climatic balance at their margins and accelerated the collapse to full Snowball, as suggested by *Goodman and Pierrehumbert* [2003]. As in earlier EBM studies [*Budyko*, 1969; *Sellers*, 1969; *Crowley et al.*, 2001], the equilibrium ice line in our model advanced gradually equatorward to $\sim 35^\circ$ as radiative cooling increased, then jumped abruptly to the equator as a consequence of ice-albedo feedback (Figure 2). Surprisingly, sea-glacier dynamics made little difference to either the equilibrium ice line or to the collapse point. The reason is that the additional heat required to melt the flowing ice at the ice margin is not supplied locally, but is instead derived from a larger range of influence of the order of $\sim 20^\circ$ latitude, as is typical of diffusive EBMs [*North*, 1984]. Thus the required adjustments to the subtropical heat transport profiles are easily accommodated and barely influence albedo feedback at the ice margin. This suggests that inclusion of ice dynamics may not significantly alter the conditions for onset of global glaciation in GCMs.

[10] Once the solution jumps to the ice-covered state at -0.7 W m^{-2} radiative forcing (corresponding to a CO_2 concentration just below present), the radiative forcing must increase to 19 W m^{-2} in order to restore ice-free conditions. This value is roughly equivalent to a CO_2 concentration of ~ 32 times the present atmospheric level (PAL), as each ~ 4 W m^{-2} increment corresponds to a doubling of CO_2 [*Schneider and Thompson*, 1981]. Most of the recovery is sudden and discontinuous with respect to radiative forcing, as required for cap carbonate formation, although the ice line recedes gradually to $\sim 10^\circ$ latitude before the main retreat (Figure 2). Sea-glacier flow does significantly delay the full recovery, which occurs at 11 W m^{-2} with no flow (not shown).

[11] The recovery value of 32 PAL of CO_2 in our thin-ice model is much lower than in our "hard Snowball" model (i.e., kilometer-thick ice everywhere; see below) which requires 55 W m^{-2} of radiative forcing, or $\sim$16,000 PAL of CO_2, to deglaciate. It is also much lower than the recovery value of 400 PAL of CO_2 in the *Caldeira and Kasting* [1992] EBM calculation. *Pierrehumbert* [2004] has published a hard-Snowball GCM calculation in which the system fails to recover even at 550 PAL (0.2 bars) of CO_2. The reason for the quicker recovery in Figure 2 is intrinsic to the behavior of thin tropical ice. As CO_2 forcing and tropical surface temperatures increase to the right along the lower branches in Figure 2, the tropical ice thins from several meters to only a few tens of centimeters. This allows more visible solar radiation to penetrate through the ice base, so that tropical broadband albedos decrease from ~ 0.45 to ~ 0.20 shortly before recovery (in contrast to the constant value of 0.663 used by *Caldeira and Kasting* [1992]). The resulting warming acts as a positive feedback for very thin ice and hastens the recovery to an ice-free world.

[12] The lower recovery value with thin ice, 32 PAL of CO_2, may imply a much shorter recovery time than the 30 Myr quoted by *Caldeira and Kasting* [1992] or the even longer timescales suggested by *Pierrehumbert* [2004]. Caldeira and Kasting's model required 400 PAL (0.12 bars) of CO_2 to deglaciate. At a CO_2 concentration of $\sim$300 ppmv, the present atmosphere contains $\sim 5 \times 10^{16}$ mol CO_2. The present release rate of CO_2 from volcanic outgassing and metamorphic degassing is $\sim 5 \times 10^{12}$ mol yr^{-1} [*Sleep and*

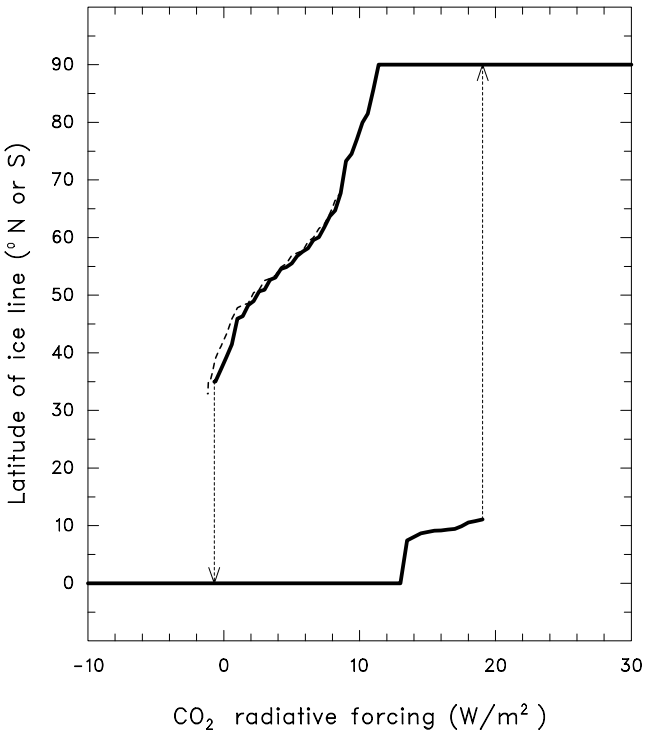

Figure 2. Latitude of the perennial ice edge versus CO_2 radiative forcing in model solutions with (solid curve) and without (dashed) sea-glacier flow. The CO_2 radiative forcing is applied as a uniform decrement to the outgoing planetary infrared radiation, representing variations in atmospheric CO_2 amount relative to today [*Hyde et al.*, 2000; *Crowley et al.*, 2001]. Here $\omega_0 = 0.994$, a value that yields thin tropical ice in full Snowball solutions. Dotted arrows show discontinuous jumps into and out of Snowball Earth with sea-glacier flow.

Zahnle, 2001; *Holland*, 2002]. The timescale for accumulating 1 PAL of CO_2 is therefore 10^4 years, assuming no exchange of gas between the atmosphere and ocean. Thus Caldeira and Kasting's model should have deglaciated in 400×10^4 years, or 4 Myr. The time required to accumulate 32 PAL of CO_2 is only ~300,000 years. However, this factor of 32 increase in CO_2 is a relative value. If atmospheric CO_2 was 2 PAL prior to the glaciation [*Hyde et al.*, 2000], well within our model uncertainty, then the timescale for deglaciating the thin ice model would be 600,000 years, again assuming no atmosphere-ocean gas exchange.

[13] The assumption that the ice forms an impermeable barrier between atmosphere and ocean is probably valid for the hard Snowball model. However, thin tropical ice would likely have been permeable to atmospheric gases because of wind-induced formation of leads (cracks), which occupy ~2% of the area in our model with sea-glacier flow, as discussed further below. Hence some transfer of CO_2 should have occurred between the atmosphere and ocean. This could lengthen the timescale for recovery in the "thin ice" model, depending on how widely that dissolved CO_2 became distributed and how the additional CO_2 was partitioned between the atmosphere and ocean. The present ocean contains ~60 times as much dissolved inorganic carbon as the atmosphere does CO_2. If this ratio remained the same as the CO_2 was absorbed, then the "thin ice" model could have required up to ~1900 PAL of outgassed CO_2 to recover (or twice that value if one starts from 2 PAL of CO_2). Accumulating this much CO_2 would require 20–40 Myr. However, these numbers are misleading because ocean chemistry would certainly change if this much CO_2 was added to it. Assuming that the ocean remained at constant alkalinity, the effect of the added CO_2 would be to convert carbonate ions into bicarbonate ions ($CO_2 + CO_3^{=} + H_2O \rightarrow 2\ HCO_3^{-}$) until the carbonate ion was exhausted, after which ocean pH would begin to decrease, and more and more of the added CO_2 would remain in the atmosphere. The ocean contains $\sim 10^{17}$ mol $CO_3^{=}$ [*Broecker and Peng*, 1982], or roughly twice the amount of CO_2 in the modern atmosphere. This suggests that the capacity of the ocean to absorb volcanic CO_2 is limited and, thus, that the recovery timescale would not be greatly lengthened by this process. Furthermore, thorough mixing of CO_2 into the ocean would imply that atmospheric O_2 was also well mixed, which is inconsistent with the reappearance of banded-iron formations. So, while the timescale for recovery remains uncertain, it may well have been relatively short.

3. Results: Full Snowball Solutions

[14] We next examined full Snowball solutions with CO_2 radiative forcing set to -3 W m^{-2} relative to the present (just below the collapse value of -0.7 W m^{-2}; the solutions are very similar for these two values). When sea-glacier flow is neglected, the ice thickness at each latitude remains in equilibrium with the local climate and ocean temperature (Figure 3). Two fundamentally different types of solutions are obtained for tropical ice thickness, h, depending on the visible single scattering albedo, ω_0: "thick ice" solutions ($h \sim$ tens to hundreds of m) for $\omega_0 > 0.995$, and "thin ice" solutions ($h \sim$ a few meters or less) for $\omega_0 < 0.995$. The latter solutions are similar to those found by *McKay* [2000], although the ice radiative transfer is handled differently in our model (see next section). Physically, low values of ω_0, corresponding to low bubble densities, allow a significant fraction of the sunlight to be transmitted. This energy must be conducted back up through the ice, which in turn forces the ice to remain thin [*McKay*, 2000]. The effect is augmented in the EBM by lower surface albedos and, hence, warmer surface temperatures for low values of ω_0.

[15] For "bubbly" ice ($\omega_0 = 0.999$), ice thicknesses are hundreds to thousands of meters everywhere, and the tropical broadband surface albedo is ~0.64 (Figure 3, dashed curves). For less bubbly "clear" ice ($\omega_0 = 0.994$), thin-ice solutions with thicknesses of ~0.2 to 1 m occur at latitudes equatorward of ~17° (Figure 3, solid curves). The latitudinal extent of thin-ice solutions is influenced by an additional factor not included in McKay's model: snow cover in higher latitudes, which prevents solar radiation from penetrating and thus forces thick ice solutions poleward of 17°, regardless of surface temperature. The very thin ice has low surface albedos (~0.20) and large lead fractions (10%), so that tropical surface temperatures and evaporation (E) are relatively high (−9°C and 70 mm yr^{-1} respectively, with net surface radiative input of ~115 W m^{-2}

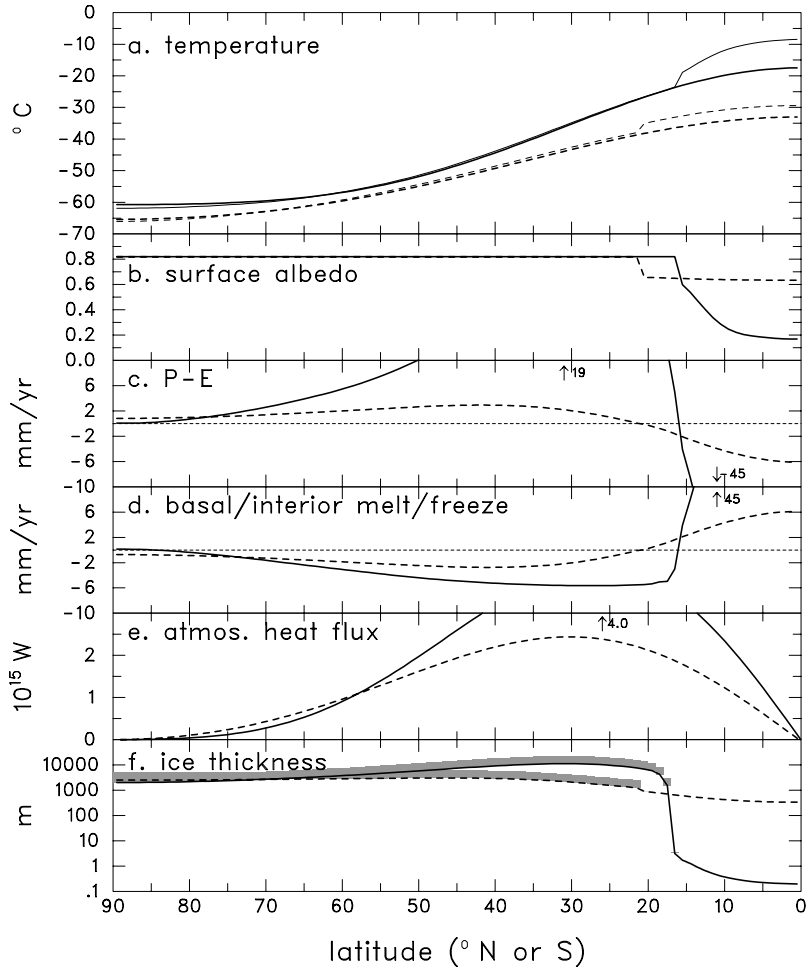

Figure 3. Latitudinal distributions of annual mean quantities in full-Snowball experiments with no sea-glacier flow. The CO_2 radiative forcing is -3 W m^{-2}, just below that needed to induce collapse to Snowball Earth. The equations were integrated for $\sim 10^6$ years to allow the thick ice to reach equilibrium. Dashed curves are for bubbly ice ($\omega_o = 0.999$), and solid curves are for relatively clear ice ($\omega_o = 0.994$). (a) Air temperature (thicker curves) and surface temperature (thinner, warmer curves). (b) Surface albedo (wave band-integrated). (c) Precipitation minus evaporation. (d) Rate of local melting (negative) or freezing (positive) at the base or interior of the ice. (e) Poleward atmospheric heat flux (including latent heat of water vapor), in Petawatts. (f) Ice thickness (logarithmic scale), with perennial snow cover indicated by shaded strips.

balanced primarily by a large upward sensible heat flux driven by $\sim$10°C surface/air temperature contrast; see Figure 3a). The resulting snowfall minus evaporation in midlatitudes is greater than the geothermal heat flux's capacity to melt basal ice, so the ice thickness grows without limit. The simulation shown in Figure 3 (solid curves) was terminated arbitrarily with $\sim$10 km ice in midlatitudes. In reality, such huge thicknesses would be prevented by lateral sea-glacier flow.

[16] When sea-glacier dynamics is turned on in the model, ice flows from high latitudes, where it is thick, toward low latitudes, where it is thinner. Surprisingly, for low ω_0, the tropical ice remains thin equatorward of $\sim$12° latitude (Figure 4, solid curves). This contradicts the expectation [*Goodman and Pierrehumbert*, 2003] that the large equatorward ice flux at the thick margin, with a velocity $\sim$800 m yr^{-1} and vertical relief of $\sim$150 m, would quickly push the thick-ice front all the way to the equator. Instead, the incoming ice mostly disappears within a few degrees latitude. The location of the transition is heavily influenced by the extent of perennial snow cover, which forces thick-ice solutions where present. Without sea-glacier flow in the low-ω_0 case, the ice immediately jumps to the thin-ice solution equatorward of the snow limit (Figure 3f, solid curve). With sea-glacier flow included, the snow limit advances slightly to 13° as a consequence of transport on top of the moving ice. More importantly, a $\sim$500 mm yr^{-1} positive convergence of ice mass in the transition region between $\sim$12° and 10° latitude thickens the bare ice to several tens of meters (Figure 4f, solid curve). These thicknesses are far out of equilibrium with local surface and basal conditions. In this same region, penetrating solar radiation produces internal ice melting of $\sim$500 mm yr^{-1} (requiring absorption of just $\sim$5 W m^{-2}, see Appendix A),

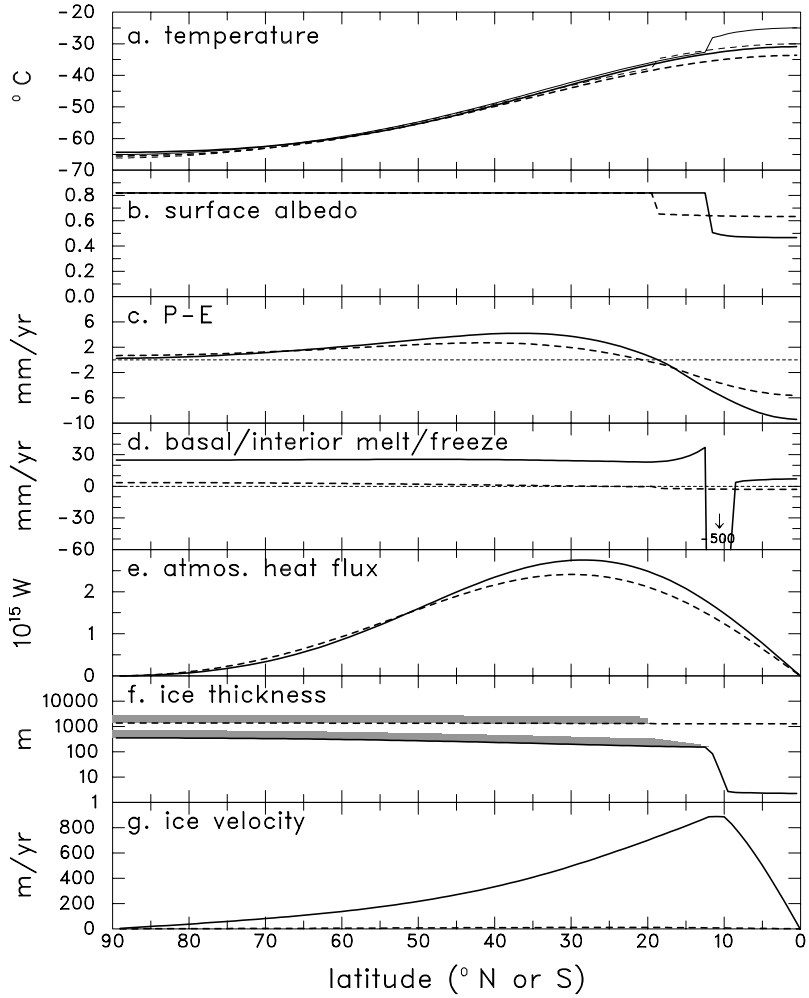

Figure 4. (a–f) As in Figure 3 except with sea-glacier flow included. (g) Equatorward ice velocity. (f and g) For the bubbly ice case (dashed curves), the latitudinal ice-thickness variations and velocities are very small but nonzero (see text).

which balances the sea-glacier mass convergence. Equatorward of this transition zone in the thin-ice solution, mass convergence due to decreasing velocities is much smaller, ~2 mm yr^{-1}, and is easily compensated by surface ablation and bottom melting.

[17] In the tropics away from the transition zone (Figure 4f, solid curve), the mass balance of the thin ice is dominated by local processes, and leads (cracks) in the ice play an important role. Lead area is parameterized as a decreasing function of ice thickness and is ~2% in the tropics where the ice thickness is ~2 m. The exposed ocean surface undergoes rapid freezing, producing new ice that balances local basal melting and surface ablation, and makes the overall ice thicker than it would be without leads. If no leads are allowed in the model, the tropical ice thins to just ~30 cm (not shown). Thus the treatment of leads and other details is important in the character of the solution, as discussed further below. The 2-m thick tropical ice in Figure 4f (solid curve) has a broadband surface albedo of ~0.45 and a transmissivity of 0.04–0.06. This is more than enough sunlight to maintain a healthy rate of photosynthesis, thereby allowing photosynthetic algae to survive the Snowball Earth.

[18] For the bubbly ice case with sea-glacier flow, thick ice is pervasive (Figure 4, dashed curves). The equator-to-pole difference in ice thickness is 85 m, and velocities are up to ~11 m yr^{-1}. These are smaller than *Goodman and Pierrehumbert*'s [2003] ~500 m and 50 m yr^{-1}, presumably due to their larger P-E magnitudes. (For our clear-ice case (Figure 4, solid curves), local budgets are dominated by basal melt/freeze, so the P-E magnitudes are unimportant.)

4. Optical Properties of Neoproterozoic Sea Ice

[19] The treatment of solar radiative transfer in ice is important, both for maintaining thin ice in the tropics and for generating internal melting of sea glaciers in the transition zone around ~10 to 12° latitude. For bubble radii of 0.1 mm, the critical value of ω_0 at which the tropical ice switches from thick to thin (0.995) corresponds to a bubble density of ~0.32 mm^{-3} (see Appendix A). These values are well within the ranges observed in the upper regions of Antarctic ice cores [*Lipenkov*, 2000]. Both there and in the sea-glacier transition zone in our model, the ice is formed by compaction of snow; hence, air bubbles are the main scatterers.

[20] In contrast, the much thinner tropical ice in our model forms locally by basal freezing of ocean water, as does modern sea ice. Here, scattering is dominated by brine inclusions. These are incorporated at the ice-water interface as ice "walls" (dendrites) that grow vertically, followed by horizontal, interbridging "floors" that seal off brine pockets [*Weeks and Ackley*, 1986; *Perovich*, 1996, 2003; *Eicken*, 2003]. However, the much slower Neoproterozoic freeze-on rates of a few mm yr^{-1} could well produce very low brine and bubble densities here as well. The freezing rate at the base of the tropical sea ice in our model is ~7 mm yr^{-1}, or 2×10^{-4} μm s^{-1}. Laboratory studies show that air bubbles essentially disappear at freezing rates <3 μm s^{-1} [*Bari and Hallett*, 1974]. There are little or no experimental or observational data on brine inclusions at such low freezing rates, but trends and theoretical studies indicate that they would either be drastically reduced or absent entirely [*Wettlaufer*, 1998; *Eicken*, 2003; *Zotikov et al.*, 1980]. Thus thin tropical ice should have been essentially bubble- and brine-free. Future laboratory work could test whether this part of our hypothesis is valid.

[21] Hence there are good reasons to expect that Neoproterozoic ice of both origins (basal freezing in the tropics, and surface accumulation at higher latitudes) could have been extremely clear. (Note that in the current model, optical properties of ice such as ω_0 are applied uniformly regardless of its origin. This dependence could be explored in future modeling work.)

[22] For completeness we performed some simulations assuming even clearer ice, i.e., ω_0 values below 0.994 (with sea-glacier flow, not shown). There is no sudden transition to ice-free tropics analogous to the thick/thin-ice transition at $\omega_0 = 0.995$, but as ω_0 is decreased, tropical ice suddenly thins to a few tens of cm at $\omega_0 \sim .992$, followed by gradual further thinning down to at least $\omega_0 \sim .980$.

5. Overall Ice Balance

[23] The planetary-scale flow of sea glaciers can be viewed in the same way as terrestrial ice sheets or glaciers, with a positive accumulation zone of snow and ice mass in high and midlatitudes, a negative ablation zone in the subtropics, and local equilibrium maintained at each point by convergence or divergence of equatorward sea-glacier flow. Here we summarize the main aspects of this balance in our thin-ice solutions.

[24] 1. As in many other climate simulations of full Snowball conditions, our model predicts net positive surface accumulation (P-E) of a few mm yr^{-1}, and hence fresh snow cover in high and midlatitudes, along with slightly higher net surface ablation, and hence bare ice, in low latitudes.

[25] 2. Ignoring sea-glacier flow for the moment, this pattern of surface mass forcing would imply ~km thick ice poleward of the snow limit (where P-E = 0), as snow cover prevents any solar radiation from penetrating. In addition, given clear enough ice, it implies McKay-type, thin-ice solutions of just a few meters thickness equatorward of the snow limit, produced by penetrating solar radiation.

[26] 3. Given standard ice rheology (based on modern observed ice-shelf and ice sheet flow, with Arrhenius allowance for Snowball Earth temperatures), a balance is reached in middle and high latitudes between equatorward sea-glacier divergence and basal freeze-on when ice thicknesses reach ~300 m. The basal freeze-on rate is then ~25 mm yr^{-1} (dominating over surface P-E) between the pole and the snow limit, assumed for these rough calculations to be at 12°. The net input is balanced by the sea-glacier flux across 12°, with an ice thickness of ~150 m moving equatorward at ~800 m yr^{-1}, i.e., $150 \times 800 \times \cos(12°) \cong 0.025$ r [1 − sin(12°)], where r is the Earth radius.

[27] 4. Just equatorward of the snow limit, there is a transition zone with ice thinning equatorward toward the thin tropical ice. Here, the bare ice is a few tens of meters thick, far out of local equilibrium due to sea-glacier convergence. The excess thickness results in ~5 W m^{-2} of penetrating solar radiation that causes internal ice melt, which follows from the ice heat equation (A11). This produces ~500 mm yr^{-1} of internal ice melt and drainage that occurs over about 2 degrees latitude (12° to 10°) and, thus, balances almost all of the sea-glacier influx at 12°, i.e., $150 \times 800 \times \cos(12°) \cong 0.500$ r [sin(12°) − sin(10°)].

6. Sensitivity Studies and Caveats

[28] In designing the nominal EBM and ice model (described more fully in Appendix A), our goal was to include a minimal, self-consistent set of physical processes that are of clear importance to sea-glacier dynamics on Snowball Earth. In hindsight, however, the nature of the solutions points to a number of model simplifications and omissions that could significantly affect the thin-ice results. For example, our model treats snow as a homogeneous substance with a density of 250 kg m^{-3} and a cold-surface broadband albedo of 0.82. The standard model assumes an arbitrary limit of 10 m on snow depth, at which point excess snow is instantaneously converted to ice. In modern glaciers and ice sheets, however, snow transforms gradually to firn and ice, and the physical and optical properties vary substantially over depths of many tens of meters [*Herron and Langway*, 1980; *Lipenkov*, 2000]. This same process of compaction and densification should occur at high and midlatitudes on Snowball Earth and could affect the properties of emerging firn as it is advected by sea-glacier flow into the subtropical ablation zone (where P-E is negative) equatorward of ~20°. If the amount of firn entering this zone is much greater than 10 m, it could potentially overwhelm the tropical thin ice. Indeed, increasing the snow depth limit in our nominal model from 10 m to 30 m, without attempting to recalculate the optical properties of the snow, causes the thin-ice solution to disappear. We show below, however, that other neglected factors (e.g., the presence of dirt) may bring it back.

[29] The meteorological effects of evaporation of ocean water through leads (cracks) in the thin tropical ice are also surprisingly important. Even with relatively light tropical winds, some leads would be expected in few-meters-thick tropical ice. The parameterization in our model predicts ~2% open tropical water, similar to the wintertime situation in the central Arctic today [*Lindsay and Rothrock*, 1995]. This allows large fluxes of sensible and latent heat [*Serreze et al.*, 1992; *Andreas and Cash*, 1999] due to the ~30°C temperature contrast between open ocean and the atmosphere (with significant effects on ice thickness as discussed

above). Our nominal model places a limit on evaporation rate for numerical stability, which may be physically unrealistic. When this restriction is relaxed by allowing for fractional lead area, the greater tropical evaporation rates cause greater snowfall in the subtropics, again allowing the snow covered, flowing sea glaciers to overwhelm nearly all tropical thin ice. In other words, the change in the Bowen ratio (the ratio of surface sensible to latent heat flux) produces enough extra snowfall to destabilize our thin-ice solution. The Bowen ratio is a difficult parameter to calculate accurately in climate models, as are interactions between convection over leads and the tropical circulation, and the resulting distribution of snowfall. More sophisticated, 3-D simulations may be needed to treat this issue realistically.

[30] A possible way of countering both of these problems, and re-establishing thin-ice solutions, is to include the effects of wind-blown dust. In Snowball Earth models with predicted terrestrial ice sheets [*Donnadieu et al.*, 2003; *Pollard and Kasting*, 2004], large continental areas remain ice-free. Wind-blown dust could have been widespread, as it was during the more recent Pleistocene ice ages. Its primary effect would have been to darken snow and ice surfaces, especially compacted firn emerging in the ablation zone, and thus to accelerate its evaporation or internal melting [cf. *Clow*, 1987]. We simulated this effect by reducing the albedo of ''emerging'' snow in the ablation zone (where P-E < 0) from 0.82 to 0.72 (and neglecting any dust effects on bare ice). This relatively small change was enough to restore the thin-ice solution in both of the sensitivity experiments described above. We conclude that wind-blown dust could have been important in deciding whether the system would have stabilized in a hard Snowball or thin-ice solution. Once again, this is an issue that would require 3-D GCM calculations to address more accurately. Even then, it would be difficult to find definitive answers, as the solution would likely depend on poorly known factors such as continental positions and topography.

[31] The above discussion applies to open-ocean conditions, where sea glaciers flow freely on hemispheric or at least oceanic scales (as assumed in our ice-flow model and in Figure 4). Large lakes and geographically confined seas such as the modern Mediterranean present an entirely different situation. (Small tropical lakes are *not* likely refugia for life, as they would have sublimated away during the course of the Snowball glaciation.) Here, sea glaciers could not have penetrated, and local ice-shelf flow would merely have helped to homogenize the ice thickness within the confines of the lake. Continental ice sheets could conceivably have flowed into such lakes, but then again continental ice sheets were localized and possibly transient phenomena during Snowball Earth episodes [*Donnadieu et al.*, 2003; *Pollard and Kasting*, 2004]. Such bodies of water can be represented crudely by the surface components of our model with no ice flow or ocean heat transport, driven at any location by the appropriate meteorology obtained from the global simulations described above. For clear ice ($\omega_0 \leq 0.994$) and using the meteorology from the simulation in Figure 4 (solid curves), we find that isolated water bodies would have thin ($\sim$2 m) ice at latitudes equatorward of 18°. This suggests that any large, isolated body of water within that zone could have acted as a refugium for photosynthetic life, even if the rest of the world was locked in a hard Snowball.

7. Conclusions

[32] Our calculations with a simple zonal mean EBM and ice model suggest that thin tropical ice solutions of the type found by *McKay* [2000] could have prevailed in full Snowball Earth, despite the equatorward flux of thick ice from higher latitudes. Our model explains the two most fundamental constraints on the Neoproterozoic glaciations, the existence of cap carbonate deposits and the survival of photosynthetic biota. It also suggests that recovery times could have been up to 100 times shorter than previous estimates (300,000 years as compared to 30 Myr), although the recovery time could be lengthened by CO_2 exchange between the atmosphere and ocean.

[33] Even if thin ice was not present in the tropical ocean, it could still have prevailed on large, low-latitude lakes and confined seas like the modern Mediterranean, protected from planetary-scale sea-glacier flow by surrounding continents. This, by itself, may have provided sufficient refugia to explain the survival of photosynthetic algae and other marine organisms. Such localized thin-ice solutions should not have been sufficiently widespread to have significantly affected the planetary albedo, however; thus, the predicted recovery time for this type of model is similar to that for the hard Snowball.

[34] Finally, as discussed in section 6, some processes that are beyond the scope of simple diffusive energy balance and homogeneous ice-flow models may in fact be important. Consequently, our thin-ice solutions may not be robust, at least for the open ocean. These processes include tropical circulation and precipitation systems induced by evaporation over leads, the amount of wind-blown dust deposited on snow covered sea glaciers as they flow toward the equator, and snow-firn metamorphosis. Sensitivity experiments with our current model show that the effects may be significant. Even a more comprehensive 3-D model, with detailed treatments of meteorological processes and other ice-surface effects discussed by *Warren et al.* [2002], may not be able to produce definitive answers, as it is virtually impossible to know how dusty the atmosphere was during these episodes. Thus the real conclusion that should be drawn from our modeling is that both hard Snowball and thin ice solutions are theoretically possible, and only a comprehensive analysis of the geological and biological evidence can tell us which type of event actually occurred.

Appendix A: Model Formulation

[35] The coupled energy-balance climate/sea-glacier model (as used in the nominal simulations in sections 2 and 3) is described here in detail. A list of parameter values is included at the end. Figures provide background information on penetrating solar radiation, internal ice melt, and sea-glacier flow.

A1. Overall Structure

[36] The model is zonally symmetric, seasonal, and applied to an all-ocean planet on a 1° latitudinal grid using a time step of 5 days. The model structure and all

prognostic variables are shown schematically in Figure 1. A single-layer atmosphere is used, as in early energy-balance climate models (EBMs, e.g., *North* [1975]). Additional explicit layers are used for snow, ice, and upper ocean, all of which exchange heat and water vertically with the atmosphere. This focus on surface detail is in line with the Snowball Earth problems we wish to investigate. Much the same approach has been taken in EBM modeling by *Maqueda et al.* [1998], *Bendtsen* [2002], and others.

A2. Atmospheric and Oceanic Horizontal Transport

[37] The single-layer atmosphere diffuses heat and water vapor latitudinally, and the single-layer ocean diffuses heat in a similar manner. The prognostic equations for atmospheric (near-surface) air temperature T_a, atmospheric specific humidity q_a, and ocean mixed-layer temperature T_o, are

$$\rho_a c_a h_a \frac{\partial T_a}{\partial t} = \frac{\partial}{\partial x}\left[\left(1-x^2\right)\rho_a c_a h_a \frac{D_a}{r^2}\frac{\partial T_a}{\partial x}\right] + Q_a + I_a + H_a + LP, \tag{A1}$$

$$\rho_a h_q \frac{\partial q_a}{\partial t} = \frac{\partial}{\partial x}\left[\left(1-x^2\right)\rho_a h_q \frac{D_q}{r^2}\frac{\partial q_a}{\partial x}\right] - (P-E), \tag{A2}$$

$$\rho_o c_o h_o \frac{\partial T_o}{\partial t} = \frac{\partial}{\partial x}\left[\left(1-x^2\right)\rho_o c_o h_o \frac{D_o}{r^2}\frac{\partial T_o}{\partial x}\right] + Q_o + I_o + H_o - LE_o + G. \tag{A3}$$

Here ρ_a and ρ_o are uniform densities for air and water respectively, c_a and c_o are air and water specific heats, h_a and h_q are atmospheric layer thicknesses for heat and moisture (~troposphere and bottom ~6000 m respectively), h_o is the ocean slab thickness (50 m), D_a, D_q and D_o are latitudinal diffusivities for atmospheric heat, atmospheric moisture, and oceanic heat, r is Earth radius, x is sin(latitude), and t is time. Other terms on the right-hand sides are described in later sections. Q_a and Q_o are net solar radiative fluxes absorbed by the atmosphere and ocean, respectively, and I_a and I_o are the same for thermal infrared radiation. H_a and H_o are sensible heat fluxes from the overall surface to the atmosphere and from the atmosphere to the ocean, respectively. P is the precipitation rate, and E and E_o are evaporation rates from the overall surface or ocean to the atmosphere, with L being the appropriate latent heat constant. G is the geothermal heat flux. Equation (A1) is solved time implicitly by spectral expansion and truncation in terms of the Legendre polynomials $P_o(x)$ to $P_4(x)$ (eigenfunctions of the diffusion operator; *North* [1975]). Equations (A2) and (A3) are solved time implicitly in physical space, using a tridiagonal solver and sub–time steps of 1 day.

[38] Precipitation rate P is parameterized as an e-folding removal of column water vapor, with the rate reduced by the degree of saturation:

$$P = \frac{\rho_a h_q q_a}{\tau_p} r_a^3, \tag{A4}$$

where r_a is atmospheric relative humidity (computed from T_a and q_a at sea level pressure), and τ_p is 12 days. Precipitation falls as snow if T_a is below 0°C. The simulated magnitudes and latitudinal profiles of precipitation are reasonable for the present, and similar to GCM results for Snowball Earth [*Pollard and Kasting*, 2004], except for Hadley Cell and ITCZ structures that depend on organized 3-D circulation.

A3. Surface Temperature of Ice or Snow

[39] Just one variable is used for the seasonally varying surface temperature T_s of bare ice or of snow on the ice. This temperature represents a thin surface layer, and is given by

$$\rho_i c_i d_i \frac{\partial T_s}{\partial t} = Q_s + I_s + H_s - LE_s + C. \tag{A5}$$

Here ρ_i is ice density, c_i is ice specific heat, and d_i is the thickness of the seasonal surface temperature wave. The product $\rho_i\, c_i\, d_i$ is assumed to be roughly appropriate for the near-surface seasonal wave in both ice and snow, with d_i = 0.5 m. Q_s and I_s are the net solar and thermal infrared radiative fluxes absorbed at the surface, H_s is the sensible heat flux from the atmosphere, E_s is evaporation rate from the ice or snow, L is the latent heat of sublimation, and C is conductive flux just below the surface, all determined as described below. Equation (A5) is solved time implicitly for T_s, using linearized Newton-Raphson terms for the emitted infrared, turbulent and conductive fluxes. If T_s becomes greater than 0°C, it is reset to 0°C and the surface-layer heat is used to melt some ice or snow, which is assumed to drain to the ocean or to temporary melt ponds.

A4. Snow and Ice Thicknesses

[40] Snow and ice thicknesses h_s and h_i vary seasonally and on longer timescales according to

$$\frac{\partial h_s}{\partial t} = S - E_s - M_s + F_s \tag{A6}$$

$$\frac{\partial h_i}{\partial t} = -E_i - M_i - M_n + F_o + F_i, \tag{A7}$$

where S is snowfall, E_s and E_i are evaporation rates from snow and ice, M_s and M_i are surface melt rates, and M_{an} is the rate of internal ice melting. F_o is the net freezing or melting rate at the ice base, determined by the difference between the conductive flux just above the base and the turbulent heat flux from the underlying ocean, plus any freezing of the ocean mixed layer itself (which may occur when the ice cover is less than 100%). F_s and F_i are longer-term horizontal convergences due to sea-glacier flow. All of these processes are calculated as described below.

[41] Fractional ice cover f_i within a grid cell is parameterized to account for leads (cracks) in thin ice. Vertical exchanges with the atmosphere are calculated separately for ice and open-ocean portions in each grid cell and averaged together to compute the net atmospheric fluxes in equations (A1) and (A2). For very thin ice (below a mean thickness of 15 cm), h_i is maintained at 15 cm for numerical stability and f_i is varied so as to conserve ice mass. For

larger h_i, f_i increases linearly from 90% at h_i = 15 cm to 100% at h_i = 3 m and above, with the exact setting of f_i again conserving ice mass. There are no leads (f_i = 1) for ice thicknesses greater than 3 m.

[42] There is no provision for fractional cover of snow; instead, the surface radiative properties (see below) trend smoothly from those of snow to those of ice as h_s decreases from 5 cm to zero. If snow depth reaches 10 m thickness, any additional snow is converted to ice at the ice-snow interface, allowing for their different densities. If the weight of snow depresses the ice-snow interface below the ocean surface, a ''white-ice'' parameterization converts some snow to ice to restore the interface to the water line.

A5. Surface Sensible and Latent Heat Fluxes

[43] Turbulent exchanges of heat and water vapor between the atmosphere and the surface (ocean, ice or snow) are computed using standard bulk transfer formulae with a uniform wind speed and corrections for static stability. Surface sensible heat fluxes are given by $\rho_a c_a C_D f_\theta \Delta T$, where ΔT is the difference in surface (T_o or T_s) and atmospheric (T_a) temperatures. (Here, ρ_a depends on air temperature, unlike in equations (A1) and (A2)). The neutral drag coefficient C_D is calculated for a ~40-m level wind speed of 5 m s^{-1} and roughness lengths of 0.0001 m for ocean or 0.001 m for ice and snow. f_θ is a correction factor for static stability depending on ΔT [*Louis*, 1979; *Pollard and Thompson*, 1995].

[44] Similarly, surface evaporation rates are given by $\rho_a C_D f_\theta \Delta q$, where Δq is the difference between atmospheric specific humidity q_a and the saturation specific humidity over water or ice, $q_{sat}(T_o)$ or $q_{sat}(T_s)$.

A6. Ocean Fluxes

[45] In addition to flux exchanges with the overlying atmosphere and horizontal heat transport, the ocean layer receives a uniform geothermal heat flux G = 0.06 W m^{-2} from below. Where covered with ice, there is a turbulent heat flux from the ocean into the bottom of the ice at a rate β ($T_o - T_m$), where β is a constant and T_m is the freezing point. Any solar radiation that penetrates all the way through the ice (see below) heats the ocean.

[46] The horizontal heat diffusion coefficient in the ocean D_o is reduced in proportion to local ice fraction f_i, and so becomes zero for 100% ice cover. This parameterization is consistent with *Poulsen*'s [2003] GCM results for a ''Slushball'' Earth, with essentially zero oceanic heat flux under the ice. If D_o is not reduced in this way, it makes little difference to our full-Snowball solutions, just shifting the transition zone between thick and thin ice a few degrees poleward. This is because our ocean temperatures under thick ice are almost exactly at the melt point, so there is essentially no diffusive heat transport under the interior ice. Whether this holds true in real oceans, with strong lateral gradients near the ice margin and no uniform geothermal heat flux, warrants further study.

A7. Atmospheric Radiative Fluxes

[47] Solar radiative fluxes through the atmosphere are treated simply as transmission, reflection, or absorption by a single atmospheric layer, accounting for multiple reflections from the underlying surface below [*Schneider and Dickinson*, 1976]. The overall atmospheric-layer transmissivity T_a, reflectivity R_a, and absorptivity A_a are 0.63, 0.24 and 0.13 respectively (cf. *Schneider*'s [1992] modern values of ~0.5, 0.25 and 0.25; our lesser absorptivity represents thinner clouds and less aerosols on Snowball Earth). The seasonal and latitudinal variations of insolation at the top of the atmosphere are computed using circular orbital geometry and a solar constant of 0.94 times today's value, appropriate for ~600 Myr ago [*Gough*, 1981].

[48] The outgoing infrared radiative flux at the top of the atmosphere is parameterized following *Thompson and Warren* [1982], who curve-fitted results of detailed radiative transfer models in terms of surface air temperature, relative humidity, and cloudiness (see *Thompson and Warren* [1982, Tables 3 and 4], assuming uniform cloudiness of 0.5 and a difference of 20°C between cloud top and surface temperatures). A uniform term is added or subtracted from the outgoing infrared radiation at all latitudes to represent variations from the present atmospheric CO_2 amount [*Hyde et al.*, 2000; *Crowley et al.*, 2001].

[49] A standard empirical expression is used for the downward infrared flux $I^\downarrow$ from the atmosphere to the surface [*Idso*, 1981; *Oke*, 1987, p. 373; *Sellers*, 1965, p. 58]:

$$I^\downarrow = \left(0.7 + 5.95\ 10^{-5} e_a e^{1500/T_a}\right)\sigma T_a^4 \left(1 + 0.2 c_l^2\right), \qquad \text{(A8)}$$

Here e_a is surface air vapor pressure (mb), T_a is surface air temperature (K), σ is the Stefan–Boltzman constant (W m^{-2} K^{-4}), and c_{al} is cloudiness fraction (0.5 here).

[50] All ocean, ice and snow surfaces are assumed to absorb and emit thermal radiation as black bodies, so the net surface upward infrared flux is $\sigma T_s^4 - I^\downarrow$ for snow or ice, and $\sigma T_o^4 - I^\downarrow$ for open ocean.

A8. Surface Radiative Fluxes

[51] Solar radiative properties of sea ice and snow are important in Snowball Earth modeling. A two-wave band treatment is used, with one band in the visible (<0.7 μm) that includes 60% of incident surface radiation, and a second in the near-infrared (>0.7 μm) that includes the remaining 40%.

[52] Some of the visible-wave band solar radiation incident on bare cold ice penetrates into the ice interior. The transmission, absorption, and reflection of visible radiation in ice are calculated here using a δ two-stream model [*Toon et al.*, 1989], described in the next section. For the near-infrared wave band, where absorption is much higher [*Warren et al.*, 2002] and where reflection is dominated by the specular component [*Mullen and Warren*, 1988], there is zero transmission into the ice. We set the near-infrared surface albedo of cold ice to 0.42 times the visible surface reflectivity from the δ two-stream model, a parameterization based on results in the work of *Allison et al.* [1993] and *Warren et al.* [2002]. These assumptions mimic to first order the behavior predicted by a full spectral reflection/multiple scattering model [*Warren et al.*, 2002].

[53] Visible and near-infrared albedos of a cold snow surface are taken as 0.9 and 0.7 respectively, with no penetration of radiation into the snow. The effects of darker surface melt ponds are included simply by linear transitions

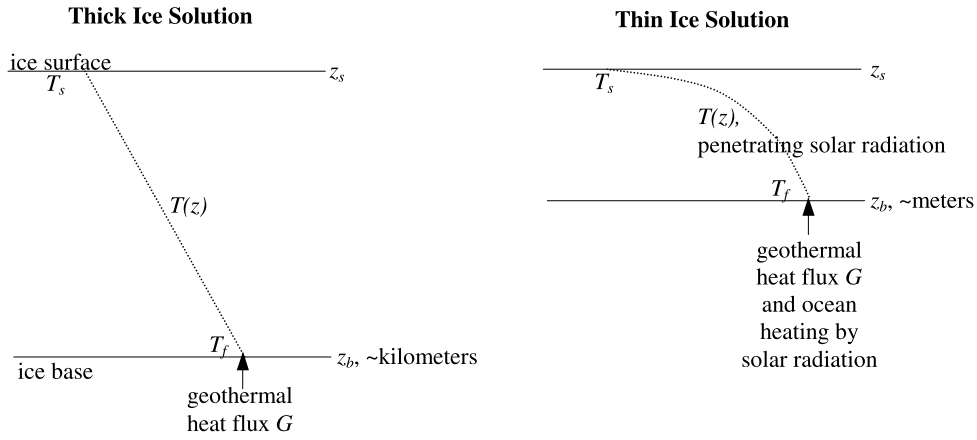

Figure A1. In a Snowball Earth with negligible sublimation or ablation at the ice-atmosphere interface and no penetrating solar radiation, the equilibrium ice thickness is determined by the need to conduct geothermal heat through the ice. The conductive heat flux is given by $F = k_i\,(dT/dz) \cong k_i(\Delta T/h_i)$, where k_i is the thermal conductivity of ice, ΔT is the temperature difference through the ice layer, and h_i is the ice thickness. The equilibrium ice thickness is thus $h_i \sim k_i\,(T_f - T_s)/G$, where T_f and T_s are the temperatures at the bottom and top of the ice, respectively. For $k_i \sim 2$ W m^{-1} K^{-1}, $T_f \sim -2$°C, $T_s \sim -40$°C and $G \sim 0.06$ W m^{-2}, this yields $h_i \sim 1.3$ km. As shown by *McKay* [2000], penetration of solar radiation can modify this equilibrium thickness drastically. A quick calculation shows why this is true. The average solar flux hitting Earth's surface in the tropics is roughly 300 W m^{-2}. About half of this radiation, or 150 W m^{-2}, is at wavelengths <700 nm where ice is relatively transparent. Call this value *S. S* is still ~2500 times greater than the geothermal heat flux. If all of this solar radiation penetrated the ice and therefore had to be conducted back out, the resulting ice thickness would be 1.3 km/2500 ≅ 0.5 m. In reality, some of the penetrating solar radiation is absorbed within the ice, and so the ice thickness calculated by this method is too thin. However, it is clear that penetration of even a fraction of the incident sunlight should thin the ice dramatically.

from the "cold" values to other values as the surface temperature T_s rises above −5 to 0°C. At 0°C, the visible and near-infrared surface albedos become 0.5 and 0.3, respectively, for ice, and 0.6 and 0.5 for snow, with no transmission below the surface. A similar linear weighting is performed for small snow thicknesses <5 cm, between the values for snow and those of the underlying ice.

A9. Penetrating Solar Radiation Into Ice

[54] The penetration of visible-wave band solar radiation into bare cold ice is essential to tropical thin-ice solutions [*McKay*, 2000], as outlined in Figure A1. The vertical profiles of transmitted, reflected and absorbed radiation are calculated here using a δ two-stream model, which is more realistic than simpler *e*-folding treatments [*McKay*, 2000], but not as accurate as more complex radiative transfer models [*Mullen and Warren*, 1988; *Warren et al.*, 2002]. The general two-stream equations [*Toon et al.*, 1989] are

$$\frac{\partial F^+}{\partial \tau} = \gamma_1 F^+ - \gamma_2 F^- - \gamma_3 F_S \omega_o e^{-\tau/\mu_o} \tag{A9}$$

$$\frac{\partial F^-}{\partial \tau} = \gamma_2 F^+ - \gamma_1 F^- + (1-\gamma_3) F_s \omega_o e^{-\tau/\mu_o}, \tag{A10}$$

where F^+ and F^- are diffusive fluxes in the upward and downward directions respectively, and F_s is the incident visible-wave band direct solar flux at the surface with zenith angle μ_o. Assuming uniform optical properties in the ice, the optical depth τ is $(k_a + k_s)\,z$, where k_a is the absorption coefficient, k_s is the scattering coefficient, and z is depth below the surface.

[55] For the quadrature scheme [*Toon et al.*, 1989], $\gamma_1 = \sqrt{3}\,[2 - \omega_o(1 + g_i)]/2$, $\gamma_2 = \omega_o\,\sqrt{3}\,(1 - g_i)/2$, and $\gamma_3 = (1 - \sqrt{3}\,g_i\,\mu_o)/2$, where g_i is the asymmetry parameter and ω_o is the single-scattering albedo. We use the δ-scaling transformation [*Joseph et al.*, 1976], for which ω_o, τ and g_i in the above expressions and equations are replaced by $(1 - g_i^2)\omega_o/(1 - \omega_o g_i^2)$, $\tau(1 - \omega_o g_i^2)$, and $g_i/(1 + g_i)$ respectively. We have corrected a known typo in the paper by *Toon et al.* [1989, equation (42)]; the sign preceding the second bracketed quantity in the expression for E_l should be a '−' rather than a '+', i.e., one should subtract the e_{4n+1} term rather than adding it.

[56] In our simulations we use $k_a = 0.1$ m^{-1}, $g_i = 0.85$ and various values for ω_o ranging between 0.994 and 0.999 (prior to the δ scaling). The value of ω_o determines k_s via the relation $\omega_o = k_s/(k_s + k_a)$. Equations (A9) and (A10) can be solved analytically for a homogeneous medium, but here the capability of numerically coupling solutions for discrete layers is used [*Toon et al.*, 1989], in anticipation of

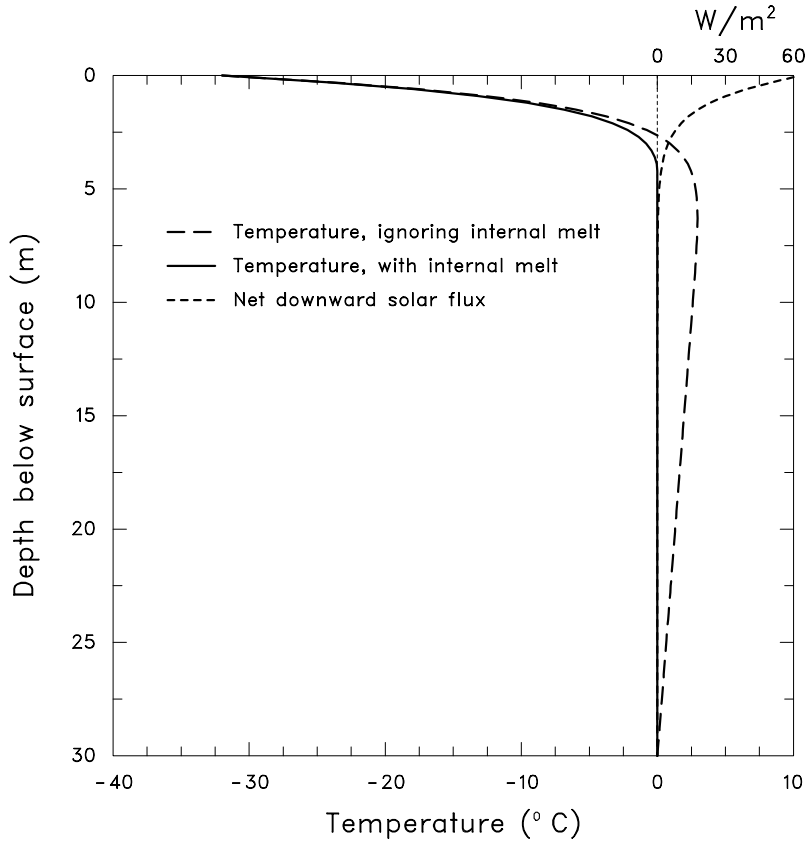

Figure A2. Vertical temperature profiles $T(z)$ in a 30-m thick ice column, showing solutions of equation (A11) with boundary conditions $T = -32°C$ at the ice surface, and 0°C at the ice base. The net downward penetrating solar radiative flux $N(z)$ is obtained from the δ two-stream equations (A9) and (A10) with ω_o =.994 and an incident surface visible-wave band solar flux of 170 W m^{-2} (60% of 283 W m^{-2}). All these conditions are typical of the thick-to-thin-ice transition zone between ∼12° and 10° latitude (see Figure 4, solid curves). Long-dashed curve: ice temperatures ignoring internal melting and the constraint $T \leq 0°C$. Solid curve: recomputed ice temperatures accounting for internal melt. Short-dashed curve: net downward penetrating solar radiation (W m^{-2}, upper scale), showing ∼2 W m^{-2} flux penetrating to the melting depth at ∼4 m. The character of these solutions and the occurrence of internal melting are affected very little by changing the basal boundary condition to $T = -2°C$, and by including a term representing sea-glacier advection of colder upstream ice.

equation (A11) (see below). The boundary conditions are $F^- = 0$ at the surface $z = 0$, and $F^+ = 0$ at the ice base $z = h_i$ assuming no reflection from the ocean. At each EBM time step and grid point with bare ice, four separate δ two-stream calculations are performed, for direct incident beams with solar zenith angles evenly distributed between 0 and 90°. The four sets of results are weighted appropriately to obtain a diurnal average, and scaled to correspond to the EBM's current downward visible-wave band flux at the surface. (The distinction between diffuse and direct incident atmospheric flux is neglected.)

[57] The nature of the solutions depends mainly on the single scattering albedo ω_o, with $\omega_o < 0.995$ needed for tropical thin ice (see main text). The critical value 0.995 corresponds to a scattering coefficient k_s of ∼20 m^{-1} (since $\omega_o = k_s/(k_s + k_a)$ and $k_a = 0.1$ m^{-1}). The scattering coefficient is related to ice properties by $k_s = 2\pi r_b^2 n_b$, where r_b and n_b are the average bubble radius and the number density of bubbles per unit volume [*Mullen and Warren*, 1988]. Bubble radii in lake ice are typically between 0.1 mm and 2 mm [*Mullen and Warren*, 1988]. Assuming r_b = 0.1 mm, then our critical ω_o value corresponds to a bubble density of 0.32 mm^{-3}.

A10. Internal Ice Temperatures and Internal Melting

[58] The δ two-stream solution includes the vertical profile of net downward penetrating radiation $N(z)$, which is used to solve for internal ice temperatures $T(z)$ via the heat conduction equation

$$k_i \frac{\partial^2 T}{\partial z^2} = \frac{\partial N}{\partial z}. \quad \text{(A11)}$$

Here, k_i is the thermal conductivity of ice, and z is measured downward from the surface. Boundary conditions are $T = T_s$ (from equation (A5)) at the surface and $T = T_m$ at the ice base. As in the work of *McKay* [2000] and *Goodman and Pierrehumbert* [2003], seasonally varying specific heat

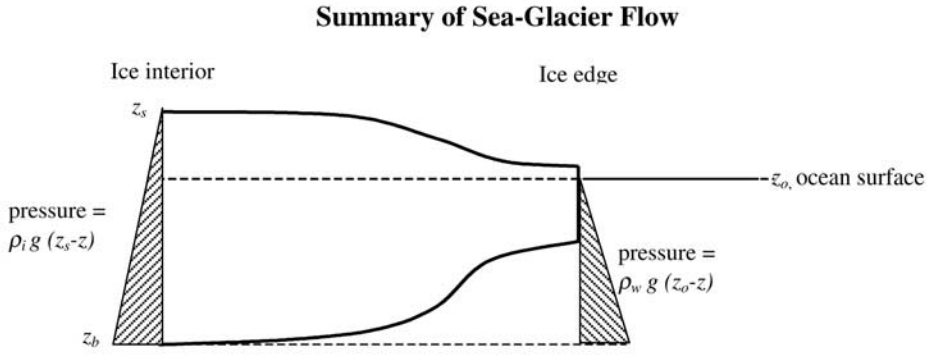

Figure A3. Floating ice with varying thickness and/or an unconfined ice edge experiences horizontal tensile stresses that tend to equalize its thickness and/or cause the ice to spread [*Weertman*, 1957]. These stresses are caused by gravity and the unequal densities of ocean water and ice. The total (vertically integrated) hydrostatic pressure in the thickest ice interior is $\int_{zb}^{zs} \rho_i g\ (z_s - z) dz = \rho_i g\ (z_s - z_b)^2/2$. Similarly, the total horizontal component of water pressure on the ice edge and sloping base is $\int_{zb}^{zo} \rho_w g\ (z_o - z)\ dz = \rho_w g\ (z_o - z_b)^2/2$. However, $\rho_i\ (z_s - z_b) = \rho_w\ (z_o - z_b)$, so the total horizontal water pressure is $(\rho_i^2/\rho_w)\ g\ (z_b - z_s)^2/2$, which is a factor of ρ_i/ρ_w less than the total interior hydrostatic pressure. The imbalance must be balanced by tensile stresses within the ice that induce stretching (horizontal velocities) away from the thick interior ice and expansion of the edge over the open ocean. Intuitively, the center of gravity of the ice-water system is lowered if the ice becomes uniformly spread over the ocean.

storage and heat advection by sea-glacier flow are neglected; the former is presumably small in the tropics, and in offline tests we have found the effect of the latter to be negligible. The solution of equation (A11) yields conductive fluxes just below the surface (needed for equations (A5)–(A7)) and just above the base (needed to determine bottom freeze/melt in equation (A7)).

[59] Given $N(z)$, an analytic solution of equation (A11) is easily derived for $T(z)$. However, the solution involves vertical integration of $N(z)$, which is performed on a discrete grid with $n_i = 20$ layers. For greater accuracy in the first few meters below the surface, unevenly spaced layers are used with thicknesses of no more than 0.5 m near the top, trending to somewhat greater than h_i/n_i at lower levels.

[60] The solution $T(z)$ is checked for internal ice temperatures above the melt point. These must occur whenever temperatures would otherwise increase upward at the base, i.e., if $\int N dz/h_i - N_b > k_i(T_m - T_s)/h_i$, where h_i is ice thickness, $\int N dz$ is the vertical integral of N from 0 to h_i, and $N_b(= N(h_i))$ is penetrating radiation at the base. In this case a new solution of equation (A11) is computed from the surface to a certain level h_m at which $T = T_m$ and $\partial T/\partial z = 0$ (and still with $T = T_s$ at the surface). The value of h_m that allows all three boundary conditions to be satisfied is found by a straightforward numerical search. At all levels below h_m to the base, the ice must be at the melt point.

[61] Penetrating downward radiation at that depth $N(h_m)$ melts ice below, which is assumed to drain instantaneously to the ocean and contribute to local ice thinning. This drainage assumption is reasonable in low latitudes with small seasonal cycles, where the ice would remain at the melt point year-round between h_m and the base. Internal melting only occurs in our model when the ice thickness is far out of local equilibrium, i.e., in a subtropical transition zone where ice thicknesses of some tens of meters are maintained by strong sea-glacier convergence (see main text). Figure A2 demonstrates ice temperature profiles and internal melting for typical boundary conditions within that zone. The melting level h_m is always a few meters below the surface, with a few W m^{-2} of solar radiation penetrating to that level.

[62] Where the ice surface is melting and/or is covered by snow, there is no penetrating solar radiation, and equation (A11) applied to the snow and ice with $N(z) = 0$ yields the standard solution with uniform conductive flux, given by $(T_m - T_s)/(h_s/k_s + h_i/k_i)$.

A11. Sea Glacier Dynamics

[63] As shown in Figure A3, thick unconfined floating ice experiences tensile stresses that induce horizontal velocities tending to equalize its thickness and causing the ice to spread. This spreading is observed today in the major Ross and Filchner-Ronne ice shelves fed by the West Antarctic Ice Sheet. Equations for the deformational ice velocities in 2-D Cartesian coordinate systems have been derived and applied to these ice shelves [e.g., *Morland*, 1987; *MacAyeal et al.*, 1996]. The fundamental stress-strain relationship (Glen's law) is the same as for land-based glaciers and ice sheets; however, for unconfined floating ice there is no basal shear stress, so lateral tensile stresses are dominant. Horizontal deformational velocities are approximately constant with depth through the ice, and are nonlocal functions of the ice thickness distribution.

[64] *Goodman and Pierrehumbert* [2003] suggested that this spreading could have been important for thick floating ice in the Neoproterozoic, and adapted the ice-shelf equations to Snowball Earth by assuming zonal symmetry and allowing for the spherical geometry at global scales. (The

term "sea glaciers" was coined by *Warren et al.* [2002] to describe this aspect of Snowball Earth). Goodman and Pierrehumbert derived a single differential equation yielding equatorward ice velocity v depending on the latitudinal ice thickness distribution h_i:

$$\frac{1}{r\sin(\theta)}\frac{\partial(v\sin(\theta))}{\partial\theta} = A\left[0.25\rho_i\left(1-\frac{\rho_i}{\rho_w}\right)g\left(h_i-\frac{B}{h_i}\right)\right]^n, \quad \text{(A12)}$$

where r is the Earth radius and θ is colatitude. A and n (= 3) are the theological coefficient and exponent in Glen's flow law, with A including the usual Arrhenius temperature dependence suitably averaged over ice depth ($A = 10^{-16}$ Pa^{-3} yr^{-1} at 0°C). g is the gravitational acceleration, and ρ_w and ρ_i are the densities of water and ice, respectively. B is a constant of integration, adjusted to satisfy boundary conditions. For nonglobal ice coverage, $B = 0$ to satisfy the force-balance boundary condition at the open ice edge. For global ice coverage, B is chosen to satisfy $v = 0$ at both North and South Poles (found in our code iteratively at each time step by Newton's Method). Numerical integration of this equation equatorward from the pole(s), using $v = 0$ as the initial boundary condition, gives ice velocity v as a function of latitude.

[65] The equatorward velocities are then used to advect ice thickness h_i in the ice mass continuity equation:

$$\frac{\partial h_i}{\partial t} + \frac{1}{r\sin(\theta)}\frac{\partial}{\partial\theta}(v\sin(\theta)h_i) = M, \quad \text{(A13)}$$

where M is the net mass gain or loss due to *local* processes in the EBM. Equation (A13) is identical to equation (A7), with M here corresponding to $-E_i - M_i - M_n + F_o$ there, and $-F_i$ there corresponding to the advective term here. In order to preserve shape and reduce spurious numerical diffusion near the ice edge, we use semi-Lagrangian transport (SLT) [*Williamson and Rasch*, 1989], with a correction to conserve global ice mass. Snow on the ice surface is carried along by the same SLT method (F_s in equation(A6)). (*Oerlemans and van der Veen* [1987] have derived some analytical solutions for uniform local forcing, against which numerical solutions of equations (A12) and (A13) can be checked.)

[66] Owing to the highly nonlinear ice rheology in equation (A12), ice velocity gradients only become appreciable for ice thicknesses of a few hundred meters or more, and are negligible for sea ice a few meters thick (although thin ice can be pushed along by contiguous thick ice). It should be noted that this gravitational flow is distinct from the motion of thin sea ice driven by surface winds and ocean currents, which is neglected here. Wind and current-driven transport is important for modern sea ice with thicknesses of a few meters or less, but is probably negligible for much thicker and stiffer ice shelves and sea glaciers.

A12. Climate-Sea Glacier Coupling

[67] The climate and sea-glacier flow models are coupled interactively, with the EBM providing local net annual surface and basal budgets used in the sea-glacier model, and with sea-glacier transport modifying the latitudinal distribution of ice thickness used in the EBM. To our knowledge this is the first climate model to be fully coupled in this way. (*Goodman and Pierrehumbert* [2003] used climate model results to drive a numerical model of sea-glacier flow, but the two models were otherwise uncoupled.)

[68] All floating ice, whether centimeters-thick seasonal ice or kilometers-thick sea glacier, is represented by one model variable for ice thickness h_i, which can be changed either by local processes in the EBM or by sea-glacier advection. The EBM and the sea-glacier components are coupled synchronously, i.e., ice velocities and semi-Lagrangian transport are stepped along with the EBM every 5 days. This tight coupling, plus the use of a single variable for all ice types, avoids numerical difficulties encountered in earlier asynchronous experiments, yet preserves sharp boundaries between thin seasonal ice and thick sea glaciers.

A13. Parameter Values

[69] All physical constants and prescribed parameter values in the nominal model are listed below, along with a few other quantities described in the notes below.

$\alpha_{s\_c\_v}$	snow albedo, cold (<5°C), visible	0.90
$\alpha_{s\_c\_n}$	snow albedo, cold (<5°C), near-infrared	0.70
$\alpha_{s\_w\_v}$	snow albedo, warm (0°C), visible	0.60
$\alpha_{s\_w\_n}$	snow albedo, warm (0°C), near-infrared	0.50
$\alpha_{i\_c\_v}$	ice albedo, cold (<5°C), visible	δ two-stream calculation
$\alpha_{i\_c\_n}$	ice albedo, cold (<5°C), near-infrared	0.42 × $\alpha_{i\_c\_v}$ (see text)
$\alpha_{i\_w\_v}$	ice albedo, warm (0°C), visible	0.50
$\alpha_{i\_w\_n}$	ice albedo, warm (0°C), near-infrared	0.30
α_o	ocean surface albedo	0.15 (see section A13.1)
A	ice rheological coefficient	10^{-16} Pa^{-3} yr^{-1} at 0°C (see section A13.2)
n	ice rheological exponent	3
A_a	atmospheric layer absorptivity	0.13
T_a	atmospheric layer transmissivity	0.63
R_a	atmospheric layer reflectivity	0.24
β	ocean-ice base heat flux coefficient	30 W m^{-2} K^{-1}
c_a	specific heat of air	1004.64 J kg^{-1} K^{-1}
c_o	specific heat of water	4218 J kg^{-1} K^{-1}
c_i	specific heat of ice	2106 J kg^{-1} K^{-1}
c_l	cloud fraction	0.5
C_D	surface-atmosphere neutral drag coefficient	(see section A13.3)
d_i	thickness of surface seasonal thermal layer	0.5 m (see section A13.4)
D_a	atmospheric heat diffusivity	1.3 × 10^6 m^2 s^{-1}
D_q	atmospheric water vapor diffusivity	1.69 × 10^6 m^2 s^{-1} (see section A13.5)
D_o	ocean heat diffusivity	2.5 × 10^4 m^2 s^{-1}
g	gravitational acceleration	9.80616 m s^{-2}
g_i	asymmetry factor (visible, δ two-stream)	0.85
ω_o	single-scattering albedo (visible, δ two-stream)	0.994 or 0.999
k_a	ice absorption coefficient (visible, δ two-stream)	0.1 m^{-1}
G	geothermal heat flux	0.06 W m^{-2}

h_a	atmospheric thickness for heat	8400 m
h_q	atmospheric thickness for water vapor	6000 m
h_o	ocean mixed layer thickness	50 m
k_s	snow thermal conductivity	0.2 W m^{-1} K^{-1}
k_i	ice thermal conductivity	2.1 W m^{-1} K^{-1} (see section A13.6)
L_f	latent heat of H_2O fusion	0.3336×10^6 J kg^{-1}
L_v	latent heat of H_2O vaporization	2.5104×10^6 J kg^{-1}
L_s	latent heat of H_2O sublimation	2.8440×10^6 J kg^{-1}
ρ_a	density of air	(see section A13.7)
ρ_o	density of liquid water	1000 kg m^{-3}
ρ_i	density of ice	900 kg m^{-3}
ρ_s	density of snow	250 kg m^{-3}
r	Earth radius	6371.22 km
σ	Stefan-Boltzmann constant	5.66961×10^{-8} W m^{-2} K^{-4}
τ_p	timescale for precipitation rate	12 days
T_m	melting/freezing point of water/ice	0°C (see section A13.8)
v_a	~40-m level wind speed	5 m s^{-1}

A13.1. Note 1

[70] The broadband solar albedo of open ocean is 0.15, somewhat higher than observed today in order to compensate roughly for the lack of (brighter) continents in the model, thus yielding global mean temperatures close to observed for modern values of solar constant and CO_2. If a lower ocean albedo (~.08) is used, then the CO_2 radiative forcing must be reduced to -10 W m^{-2} to achieve full Snowball; however, the results with $\alpha_o = 0.15$ shown in Figure 2 are probably more representative of worlds with large continents.

A13.2. Note 2

[71] The ice rheological constant $A = A_o$, the value given above, is multiplied by a standard Arrhenius temperature-dependent term $\exp[(Q/R)\ (1/T_m - 1/T)]$, where $Q = 9.545 \times 10^4$ or 7.820×10^4 J mol^{-1} for ice temperatures warmer or colder than -6.5°C respectively, R is 8.314 J mol^{-1} K^{-1}, T_m is 273.16 K and T is ice temperature (K), suitably averaged over ice depth [*Ritz et al.*, 1997].

A13.3. Note 3

[72] The neutral drag coefficient C_D is $v_a\ [k/\ln(z_a/z_o)]^2$, where $k = 0.4$ is the von Karman constant, v_a is the wind speed at reference height (taken as 5 m s^{-1}), z_a is the reference height (at atmospheric σ level 0.995, ~40 m), and z_o is the surface roughness length, 0.0001 m for ocean and 0.001 m for snow and ice [*Brutsaert*, 1982].

A13.4. Note 4

[73] The product $\rho_i\ c_i\ d_i$ is used in equation (A5) for both sea-ice and snow surfaces, so the effective seasonal depth for snow is roughly ρ_i/ρ_s times greater than d_i, i.e., ~1.8 m, in agreement with *Brandt and Warren* [1997].

A13.5. Note 5

[74] D_q is set slightly larger than D_a in order to avoid negative precipitation minus evaporation on snow in small regions near the poles.

A13.6. Note 6

[75] If instead we use a temperature-dependent ice conductivity $k_i = 780/T_{ice} - 0.615$ W m^{-1} K^{-1} [*McKay*, 2000], the resulting increase in k_i leads to less internal ice melt and prevents tropical thin ice. One way to compensate is to slightly reduce the visible single scattering albedo ω_o from 0.994 to 0.993, which recovers the thin-ice solutions.

A13.7. Note 7

[76] In equations (A1) and (A2), a uniform representative value of ρ_a is used, equal to p_a/R_aT^* where $R_a = 287.04$ J kg^{-1} K^{-1}, $p_a = 10^5$ Pa, and T^* is 287 K, in order to avoid latitudinal variations inside the diffusion terms. In the calculation of surface turbulent fluxes, $\rho_a (= p_a/R_at_a)$ is allowed to depend on the local air temperature T_a.

A13.8. Note 8

[77] The melting point of ice and the freezing point of ocean water are both taken as 0°C, despite the latter's real value of approximately -2°C due to salinity. This simplifies conservation of global heat in the model.

[78] **Acknowledgments.** We thank Stephen Warren for insightful discussions on modeling radiation in ice and for sharing ongoing work in this area. We also thank an anonymous reviewer, Stephen Warren, and Jason Goodman for careful reviews. This work was supported in part by NASA Exobiology grant NAG-5-12352.

References

Allison, I., R. E. Brandt, and S. G. Warren (1993), East Antarctic sea ice: Albedo, thickness distribution, and snow cover, *J. Geophys. Res.*, *98*(C7), 12,417–12,429.

Andreas, E. L., and B. A. Cash (1999), Convective heat transfer over wintertime leads and polynyas, *J. Geophys. Res.*, *104*(C11), 25,721–25,734.

Bari, S. A., and J. Hallett (1974), Nucleation and growth of bubbles at an ice-water interface, *J. Glaciol.*, *13*, 489–520.

Bendtsen, J. (2002), Climate sensitivity to changes in solar radiation in a simple coupled climate model, *Clim. Dyn.*, *18*, 595–609.

Brandt, R. E., and S. G. Warren (1997), Temperature measurements and heat transfer in near-surface snow at the South Pole, *J. Glaciol.*, *43*, 339–351.

Broecker, W. S., and T.-H. Peng (1982), *Tracers in the Sea*, Lamont--Doherty Earth Observatory, Palisades, N. Y.

Brutsaert, W. (1982), *Evaporation Into the Atmosphere*, 299 pp., Springer, New York.

Budyko, M. I. (1969), The effect of solar radiation variations on the climate of the Earth, *Tellus*, *21*, 611–619.

Caldeira, K., and J. F. Kasting (1992), Susceptibility of the early Earth to irreversible glaciation caused by carbon dioxide clouds, *Nature*, *359*, 226–228.

Clow, G. D. (1987), Generation of liquid water on Mars through the melting of a dusty snowpack, *Icarus*, *72*, 95–127.

Crowley, T. J., W. T. Hyde, and W. R. Peltier (2001), CO_2 levels required for deglaciation of a "Near-Snowball" Earth, *Geophys. Res. Lett.*, *28*, 283–286.

Donnadieu, Y., F. Fluteau, G. Ramstein, C. Ritz, and J. Besse (2003), Is there a conflict between the Neoproterozoic glacial deposits and the snowball Earth interpretation?: An improved understanding with numerical modeling, *Earth Planet. Sci. Lett.*, *208*, 101–112.

Donnadieu, Y., Y. Godderis, G. Ramstein, A. Nedelec, and J. Meert (2004a), A "snowball Earth" climate triggered by continental break-up through changes in runoff, *Nature*, *428*, 303–306.

Donnadieu, Y., G. Ramstein, F. Fluteau, D. Roche, and A. Ganopolski (2004b), The impact of atmospheric and oceanic heat transports on the sea ice-albedo instability during the Neoproterozoic, *Clim. Dyn.*, *22*, 293–306.

Eicken, H. (2003), From the microscopic to the macroscopic to the regional scale: Growth, microstructure and properties of sea ice, in Sea Ice: An introduction to its physics, biology, chemistry and geology, edited by D. Thomas and G. S. Dieckmann, pp. 22–81, Blackwell Sci., Malden, Mass.

Evans, D. A., N. J. Beukes, and J. L. Kirshvink (1997), Low-latitude glaciation in the Proterozoic era, *Nature*, *386*, 262–266.

Goodman, J. C., and R. T. Pierrehumbert (2003), Glacial flow of floating marine ice in "Snowball Earth," *J. Geophys. Res.*, *108*(C10), 3308, doi:10.1029/2002JC001471.

Gough, D. O. (1981), Solar interior structure and luminosity variations, *Solar Phys.*, *74*, 21–34.

Halverson, G. P., A. C. Maloof, and P. F. Hoffman (2004), The Marinoan glaciation (Neoproterozoic) in northeast Svalbard, *Basin Res.*, *16*, 297–324.

Herron, M. M., and C. C. Langway (1980), Firn densification: An empirical model, *J. Glaciol.*, *25*, 379–385.

Hoffman, P. F., and D. P. Schrag (2000), Snowball Earth, *Sci. Am.*, *282*, 62–75.

Hoffman, P. F., and D. P. Schrag (2002), The Snowball Earth hypothesis: Testing the limits of global change, *Terra Nova*, *14*, 129–155.

Hoffman, P. F., A. J. Kaufman, G. P. Halverson, and D. P. Schrag (1998), A Neoproterozoic Snowball Earth, *Science*, *281*, 1342–1346.
Holland, H. D. (2002), Volcanic gases, black smokers, and the Great Oxidation Event, *Geochim. Cosmochim. Acta*, *66*, 3811–3826.
Hyde, W. T., T. J. Crowley, S. K. Baum, and W. R. Peltier (2000), Neoproterozoic "Snowball Earth" simulations with a coupled climate/ice-sheet model, *Nature*, *405*, 425–429.
Idso, S. B. (1981), A set of equations for full spectrum and 8–14 μm and 10.5–12.5 μm thermal radiation from cloudless skies, *Water Resour. Res.*, *17*, 295–304.
Jenkins, G. S. (2000), Global climate model high-obliquity solutions to the ancient climate puzzles of the Faint-Young Sun paradox and low-altitude Proterozoic glaciation, *J. Geophys. Res.*, *105*(D6), 7357–7370.
Jiang, G., M. J. Kennedy, and N. Christie-Blick (2003), Stable isotopic evidence for methane seeps in Neoproterozoic postglacial cap carbonates, *Nature*, *426*, 822–826.
Joseph, J. H., W. J. Wiscombe, and J. A. Weinman (1976), The delta-Eddington approximation for radiative transfer, *J. Atmos. Sci.*, *33*, 2452–2459.
Kennedy, M. J., N. Christie-Blick, and L. E. Sohl (2001), Are Proterozoic cap carbonates and isotopic excursions a record of gas hydrate destabilization following Earth's coldest intervals?, *Geology*, *29*, 443–446.
Kirschvink, J. L. (1992), Late Proterozoic low-latitude global glaciation: The snowball Earth, in *The Proterozoic Biosphere: A Multidisciplinary Study*, edited by J. W. Schopf and C. Klein, pp. 51–52, Cambridge Univ. Press, New York.
Knoll, A. H. (2003), *Life on a Young Planet: The First Three Billion Years of Evolution on Earth*, Princeton Univ. Press, Princeton, N. J.
Lindsay, R. W., and D. A. Rothrock (1995), Arctic sea ice leads from advanced very high resolution radiometer images, *J. Geophys. Res.*, *100*(C3), 4533–4544.
Lindzen, R. S., and B. Farrell (1977), Some realistic modifications of simple climate models, *J. Atmos. Sci.*, *34*, 1487–1500.
Lipenkov, V. Y. (2000), Air bubbles and air-hydrate crystals in the Vostok ice core, in *Physics of Ice Core Records*, edited by T. Hondoh, pp. 327–358, Hokkaido Univ. Press, Sapporo, Japan.
Louis, J. F. (1979), A parametric model of vertical eddies in the atmosphere, *Boundary Layer Meteorol.*, *17*, 187–202.
MacAyeal, D. R., V. Rommelaere, P. Huybrecht, C. L. Hulbe, J. Determann, and C. Ritz (1996), An ice-shelf model test based on the Ross Ice Shelf, Antarctica, *Ann. Glaciol.*, *23*, 46–51.
Maqueda, M. A. M., A. J. Willmott, J. L. Bamber, and M. S. Darby (1998), An investigation of the small ice cap instability with a coupled atmosphere-sea ice-ocean-terrestrial ice model, *Clim. Dyn.*, *14*, 329–352.
McKay, C. P. (2000), Thickness of tropical ice and photosynthesis on a snowball Earth, *Geophys. Res. Lett.*, *27*, 2153–2156.
Morland, L. W. (1987), Unconfined ice-shelf flow, in Dynamics of the West Antarctic Ice Sheet, edited by C. J. van der Veen and J. Oerlemans, pp. 99–116, Springer, New York.
Mullen, P. C., and S. G. Warren (1988), Theory of the optical properties of lake 111ice, *J. Geophys. Res.*, *93*(D7), 8403–8414.
North, G. R. (1975), Theory of energy-balance climate models, *J. Atmos. Sci.*, *32*, 2033–2043.
North, G. R. (1984), The small ice-cap instability in diffusive climate models, *J. Atmos. Sci.*, *41*, 3390–3395.
Oerlemans, J., and C. J. van der Veen (1987), *Ice Sheets and Climate*, 217 pp., Springer, New York.
Oke, T. R. (1987), *Boundary Layer Climates*, 2nd ed., 435 pp., Methuen, New York.
Perovich, D. K. (1996), *The Optical Properties of Sea Ice*, *Cold Reg. Res. Eng. Lab. Monogr. 96-1*, 24 pp., U.S. Army Corps of Eng., Hanover, N. H.
Perovich, D. K. (2003), Complex yet translucent: The optical properties of sea ice, *Physica B*, *338*, 107–114.
Pierrehumbert, R. T. (2004), High levels of atmospheric carbon dioxide necessary for the termination of global glaciation, *Nature*, *429*, 646–649.
Pollard, D., and J. F. Kasting (2004), Climate-ice sheet simulations of Neoproterozoic glaciation before and after collapse to Snowball Earth, in *The Extreme Proterozoic: Geology, Geochemistry, and Climate*, *Geophys. Monogr. Ser.*, vol. 146, edited by G. Jenkins et al., pp. 91–105, AGU, Washington D. C.
Pollard, D., and S. L. Thompson (1995), Use of a land-surface-transfer scheme (LSX) in a global climate model: The response to doubling stomatal resistance, *Global Planet. Change*, *10*, 129–161.
Poulsen, C. J. (2003), Absence of a runaway ice-albedo feedback in the Neoproterozoic, *Geology*, *31*, 473–476.
Poulsen, C. J., R. T. Pierrehumbert, and R. L. Jacob (2001), Impact of ocean dynamics on the simulation of the Neoproterozoic "Snowball Earth," *Geophys. Res. Lett.*, *28*, 1575–1578.
Ridgewell, A. J., M. J. Kennedy, and K. Caldeira (2003), Carbonate deposition, climate stability, and Neoproterozoic ice ages, *Science*, *302*, 859–862.
Ritz, C., A. Fabre, and A. Letreguilly (1997), Sensitivity of a Greenland ice sheet model to ice flow and ablation parameters: Consequences for the evolution through the last climatic cycle, *Clim. Dyn.*, *13*, 11–24.
Schneider, S. H. (1992), Introduction to climate modeling, in Climate System Modeling, edited by K. E. Trenberth, pp. 3–26, Cambridge Univ. Press, New York.
Schneider, S. H., and R. E. Dickinson (1976), Parameterization of fractional cloud amounts in climate models; the importance of multiple reflections, *J. Appl. Meteorol.*, *15*, 1050–1056.
Schneider, S. H., and S. L. Thompson (1981), Atmospheric CO_2 and climate: Importance of the transient response, *J. Geophys. Res.*, *86*(C4), 3135–3147.
Sellers, W. D. (1965), *Physical Climatology*, 272 pp., Univ. of Chicago Press, Chicago, Ill.
Sellers, W. D. (1969), A climate model based on the energy balance of the Earth-atmosphere system, *J. Appl. Meteorol.*, *8*, 392–400.
Serreze, M. C., J. A. Maslanik, M. C. Rehder, R. C. Schnell, J. D. Kahl, and E. L. Andreas (1992), Theoretical heights of buoyant convection above open leads in the winter Arctic pack ice cover, *J. Geophys. Res.*, *97*, 9411–9422.
Sleep, N. H., and K. Zahnle (2001), Carbon dioxide cycling and implications for climate on ancient Earth, *J. Geophys. Res.*, *106*, 1373–1399.
Thompson, S. L., and S. G. Warren (1982), Parameterization of outgoing infrared radiation derived from detailed radiative calculations, *J. Atmos. Sci.*, *39*, 2667–2680.
Toon, O. B., C. P. McKay, T. P. Ackerman, and K. Santhanam (1989), Rapid calculation of radiative heating rates and photodissociation rates in inhomogeneous multiple-scattering atmospheres, *J. Geophys. Res.*, *94*(D13), 16,286–16,301.
Warren, S. G., R. E. Brandt, T. C. Grenfell, and C. P. McKay (2002), Snowball Earth: Ice thickness on the tropical ocean, *J. Geophys. Res.*, *107*(C10), 3167, doi:10.1029/2001JC001123.
Weeks, W. F., and S. F. Ackley (1986), The growth, structure, and properties of sea ice, in *The Geophysics of Sea Ice*, *NATAO ASI Ser. B Phys.*, vol. 146, edited by N. Entertainer, pp. 9–164, Springer, New York.
Weertman, J. (1957), Deformation of floating ice shelves, *J. Glaciol.*, *3*, 38–42.
Wettlaufer, J. S. (1998), Introduction to crystallization phenomena in natural and artificial sea ice, in *Physics of Ice Covered Seas*, edited by M. Lepparanta, pp. 105–194, Helsinki Univ. Press, Helsinki.
Williamson, D. L., and P. J. Rasch (1989), Two-dimensional semi-Lagrangian transport with shape-preserving interpolation, *Mon. Weather Rev.*, *117*, 102–129.
Zotikov, I. A., V. S. Zagorodnov, and J. V. Raikovsky (1980), Core drilling through the Ross Ice Shelf (Antarctica) confirmed basal freezing, *Science*, *207*, 1463–1465.

J. F. Kasting and D. Pollard, Department of Geosciences, Earth and Environmental Systems Institute, Pennsylvania State University, University Park, PA 16802, USA. (kasting@essc.psu.edu; pollard@essc.psu.edu)